Application of a New Type of Air and Vapor Retarder in a Self-Drying Sloped Roof with a Cathedral Ceiling

Hugo Hens, Ph.D.
Member ASHRAE

Arnold Janssens, Dr.IR.

ABSTRACT

In cool and cold climates, sloped roofs with cathedral ceilings are quite sensitive to moisture damages caused by built-in moisture and prolonged concealed condensation of water vapor produced inside. Conventional solutions are to leave a cavity between the thermal insulation and the sheathing and vent it with outside air and/or to include a vapor barrier below the insulation layer. An alternative, however, is the self-drying roof. This concept was evaluated experimentally. For that purpose, three well insulated roof sections, all covered with shingles and lined inside with a gypsum board, were tested in a hot box. The first had an airflow- and vapor-tight polyethylene film between the glass fiber insulation and the gypsum board internal lining. The second had the gypsum board only as an airflow retarder, and the third had a new type of organic, glass-fiber, fabric reinforced felt as airflow and vapor retarder. The plywood deck under the shingles contained a known amount of built-in moisture. The sections were exposed to a sunny period first, followed by a steady-state cold period afterwards. Section 1 remained wet, with the moisture moving from the plywood to the polyethylene during the sunny period and back to the plywood during the cold period. Section 2 dried during the sunny period but turned wet again during the cold period. Section 3 finally dried during the sunny period and got some wetness during the cold period; however, it got less than roof 2. Apparently, roof 3 came closest to the concept of self drying.
In order to evaluate to what extent simple engineering tools and simplified models could predict the measured response, the tests were also simulated using three such models.

INTRODUCTION

In cool and cold climates, sloped roofs with cathedral ceilings are quite sensitive to moisture damage. As many authors state, main causes of the problem are built-in moisture and prolonged concealed condensation of water vapor produced inside (Rose 1994; TenWolde and Carll 1992; Cunningham et al. 1994). A conventional solution to that problem is to leave an air space between the thermal insulation and the roof sheathing and to vent it with outside air (Rose 1995). This should enhance the vapor egress in order to prevent condensation against the sheathing. Hence, research results indicate that outside air venting may aggravate instead of eliminate the condensation problem in cool, damp climates. In fact, the humid outside air becomes a vapor source itself each time clear sky radiation lowers the sheathing temperature below the outside dew point (Künzel and Grosskinsky 1989; Hens et al. 1992). Another solution, which can be used in combination with a vented air space, is to provide a vapor retarder at the inside of the insulation layer. This should reduce vapor ingress by diffusion to a harmless minimum.

An alternative for both is the self-drying roof concept (Desjarlais 1995). The performances needed to deserve this name are that moisture in the roof should not accumulate with time and that the yearly peak in moisture presence at the end of the winter should not pass beyond a harmless limit. The first restriction underlines that summer drying must compensate for winter wetting. This is only possible if the annual average of the vapor concentration inside does not pass a certain limit value. That limit value depends on those of the exterior climate (Sanders 1996). The second restriction is that vapor inflow should be retarded to such extent that winter condensation is kept below a limit of acceptability. This demands elimination of vapor inflow by convection as well as a vapor retarding quality that allows drying in warm weather without promoting too much condensation in cold weather.

In this paper, an experimental hot box testing program is described, which shows that a humidity-controlled airflow

Hugo Hens is a professor and **Arnold Janssens** is a researcher in the Department of Civil Engineering, Laboratory of Building Physics at the University Leuven, Leuven, Belgium.

and vapor retarder may help in turning the self-drying roof concept into practice. Also, some modeling exercises in relation to the tests with simple engineering tools and a simplified model are discussed.

MOISTURE PROPERTIES OF THE HUMIDITY-CONTROLLED RETARDER

The retarder consists of a cellulose-based felt, reinforced with a glass fiber fabric and coated with a thin layer of polyethylene and latex. Ammonium salts are added to upgrade the fire-retarding properties. Testing showed that the felt is quite hygroscopic. Capillary ingress appeared to be much more parallel than orthogonal to the surface. At capillary saturation, the total moisture uptake reached 0.23 kg/m^2. The ammonium salts dissolve in a humid felt and migrate to the drying front where they crystallize. This substantially modifies the sorption behavior and the specific moisture content of the felt. If wetness stays for a long time, the felt looses dimensional stability and strength, while fungal defacement becomes obvious beyond 93% relative humidity. On the other hand, independent of moisture ratio, air permeability lies between one-thirteenth of and 2 times the values measured for gypsum board. ASHRAE and NRC both indicate an air exfiltration below 0.2 L/(m^2·s) at an air pressure difference of 75 Pa as "sufficient air tight." In the case being, the felt itself guarantees an exfiltration below 0.072 L/(m^2·s) at 75 Pa. Vapor permeance is finally humidity controlled, with low values at low relative humidity, a linear increase of the permeance beyond 36%, and a very high value at high relative humidity. Also see the paper by Hens (1997) and Table 1. Recent measurements, however, suggest that alternating moistening and drying pushes the low relative humidity vapor permeance to higher values. This may degrade the humidity-related diode effect of the felt (Künzel and Grosskinsky 1997).

EXPERIMENTAL PROGRAM

Test Roofs

In General. The hot box experimental program was set up to evaluate the effectiveness of the new felt as a humidity-controlled vapor retarder in self-drying, cathedralized roof construction. Three shingle-covered roof designs were tested, the first one with an absolute polyethylene airflow and vapor retarder between the thermal insulation and the gypsum board internal lining, the second one without vapor retarder, and the third one with the felt as airflow and vapor retarder. The area of each section was 2.14 m × 0.78 m and the slope from horizontal 60°. A section consisted of three rafters 40 mm × 200 mm, with the centerlines 340 mm to 370 mm apart. They were separated from each other by a double rafter with a vapor-tight bituminous layer in between. The plywood decks of the three roof sections were conceived to be detachable in order to measure the weekly changes in weight of all layers. Before the tests started, the plywood was wetted by immersion as to simulate a situation of a high initial moisture content. After one week of immersion, the plywood deck of Section 1 attained a moisture ratio of 39.8% by weight, the plywood deck of Section 2 a moisture ratio of 44.1% by weight, and the plywood deck of Section 3 a moisture ratio of 42.5% by weight.

Section 1. See Figure 1. To the outside:

- 12.5 mm-thick gypsum board screwed to the rafters, all edges closed with silicones;
- airflow- and vapor-tight polyethylene film, thickness 0.2 mm;
- mineral fiber, thickness 20 cm, density 18 kg/m^3, composed of two layers of 10 cm each mounted with alternating joints;
- plywood deck, thickness 12.5 mm; and
- bituminous layer, covered with shingles.

TABLE 1
Air- and Vapor-Retarding Felt, Measured Moisture Properties

Property	Units	Value
Weight per m^2	kg/m^2	0.207
Sorption	% kg/kg ϕ in –	$X_H = \dfrac{\phi}{-0.2924\phi^2 + 0.314\phi - 0.0182}$ $(0.15 < \phi < 0.95)$
Desorption (After Immersion/Desalting)		$X_H = \dfrac{\phi}{-0.3159\phi^2 + 0.371\phi - 0.0279}$ $(0.15 < \phi < 0.95)$
Buffer Capacity	kg/m^2	0.22 à 0.24 kg/m^2
Vapor Permeance (New Felt)	kg/(m^2·Pa·s)	$\phi \le 0.364$ $\quad 4.1\times10^{-11}$ $\phi > 0.364$ $\quad 2.610^{-10} + 3.310^{-9}\,(\phi - 0.43)$
Air Permeance	kg/(m^2·Pa·s)	$2\times10^{-6}\Delta P_a^{-0.13}$ or 1.5×10^{-6} kg/(m^2·Pa·s) at 10 Pa

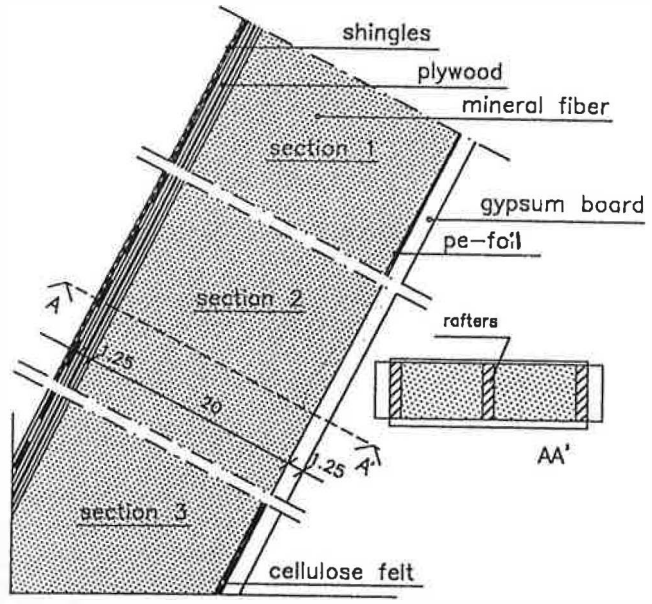

Figure 1 The three roof sections.

Sections 2 and 3. Section 2 is identical to Section 1 except that no vapor retarder is provided between the gypsum board and the mineral fiber. In Section 3, the felt replaces the polyethylene film.

Measuring Points per Section. In all three sections, temperatures were measured in all interfaces between successive layers at distances along the pitch of 23 cm, 69 cm, 107 cm, 145 cm, and 195 cm from the bottom, using copper-constantan thermocouples. Heat fluxes, in turn, were logged at both sides of the roofs at distances along the pitch of 47 cm, 107 cm, and 172 cm from the bottom, using calibrated heat flowmeter disks. Air pressures were measured at both sides of the thermal insulation at distances along the pitch of 47 cm, 107 cm, and 172 cm from the bottom, using pressure tubes. Moisture ratios were finally measured in the central rafter close to the plywood deck at distances along the pitch of 47 cm, 107 cm, and 172 cm from the bottom, using resistance pins.

Thermal and Moisture Properties of the Different Layers

Table 2 lists the thermal conductivity of the mineral fiber, the thermal conductivity of the plywood, and the thermal resistance of the gypsum board, as measured at different temperatures and different moisture ratios within a heat flowmeter apparatus. The table also gives the vapor permeance of the polyethylene film, measured with a cup test, its air permeance, and the vapor permeability and air permeance of gypsum board.

Measuring Scheme

As shown in Figure 2, the test roofs are mounted between a hot and a cold box that simulate inside and outside conditions, respectively. The experiment included two stages. During stage one, which took six weeks, a summer period was simulated with a constant cold box temperature of 22°C and solar gains each week from Monday to Friday between 8:30 a.m. and 3:30 p.m. For that purpose, we positioned a solar simulator with 30 infrared bulbs of 250 W each at such a distance from the roofs that the temperature on the shingles reached 70°C. At the same time, the hot box was kept at 22°C, 35% relative humidity, and not pressurized. The second stage simulated an average winter period of six weeks as recorded in Ukkel, Belgium: 2°C and 90% relative humidity in the cold box; 22°C, 50% relative humidity, and a 30 Pa pressurization

TABLE 2
Measured Properties of the Different Materials Used in the Test Roofs

Material	Property	Units	Value
Mineral Fiber	Density	kg/m^3	17.8
	Thermal Conductivity	W/(m·K) θ in °C	$0.033 + 0.000123\theta$ $0 < \theta < 30$°C
Plywood	Density	kg/m^3	765
	Thermal Conductivity	W/(m·K) θ in °C	$0.122 + 4.9\times10^{-3}X + 1.8\times10^{-4}\theta + 1.6\times10^{-5}$ $0 < \theta < 30$°C, $0 < X < 5$%kg/kg
PE-Foil	Vapor Permeance	$kg/(m^2\cdot Pa\cdot s)$	$1.39\times10^{-12} + 1.3\times10^{-14}\exp(7.56\phi)$ $0.25 < \phi < 0.92$
	Air Permeance	$kg/(m^2\cdot Pa\cdot s)$	5.5×10^{-11}
Gypsum Board	Weight per m^2	kg/m^2	8.0
	Thermal Resistance	$m^2\cdot K/W$	$1/(6.51 + 0.685X + 5.1\times10^{-3}\theta - 6.2\times10^{-4}X$ $0 < \theta < 30$°C, $0 < X < 18$%kg/kg
	Vapor Permeability	$kg/(m\cdot Pa\cdot s)$	$1.3\times10^{-11} + 5.2\times10^{-13}\exp(4.1\phi)$
	Air Permeance	$kg/(m^2\cdot Pa\cdot s)$	2×10^{-5} to 7.4×10^{-7} at 10 Pa

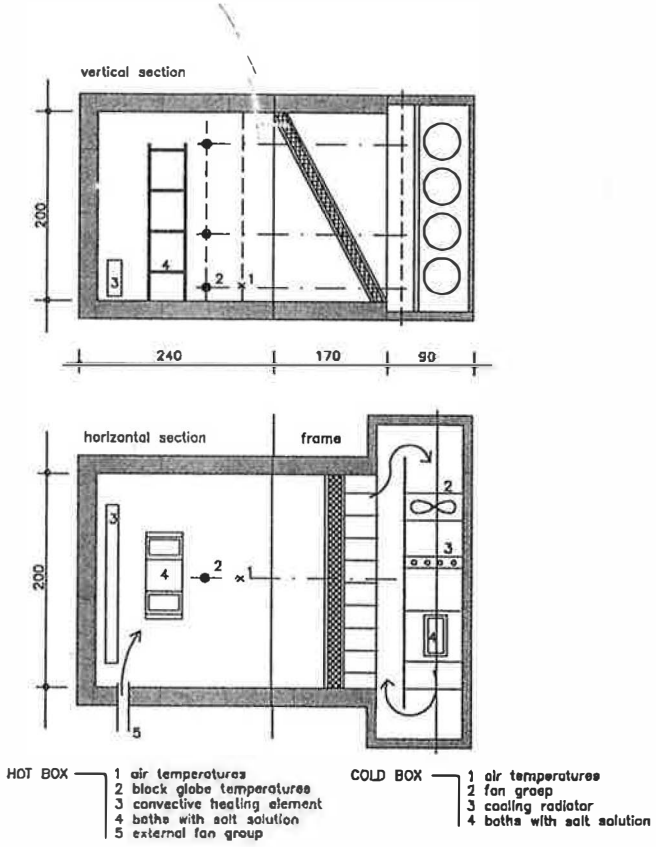

Figure 2 *Hot and cold box.*

in the hot box. That high air-pressure difference was chosen to simulate a most negative case, the combination of a fan-driven ventilation system, stack effect, and wind-driven pressure difference in a two-story living space.

Temperatures and heat fluxes were logged continuously. The moisture ratio in the central rafter of each roof and the air pressures during stage 2 were measured at the end of each week. Moisture migration through the structure was mapped weekly by weighting the plywood deck, the insulation, a loose-fill piece of the central rafter in contact with the plywood at 134 cm from the bottom, a loose-fill piece of the central rafter just above the inside lining at 76 cm from the bottom, and a blotting paper of 0.1 m^2 × 0.2 m^2, which was fixed on the vapor retarder (Sections 1 and 3) or on the internal lining (Section 2) at 102 cm from the bottom. In stage 2, a tracer gas measurement delivered information on the air permeance of the three sections.

Air Permeance of the Three Sections

In stage 2, the winter period, the tracer gas SF_6 was injected in the hot box during two hours to maintain a constant concentration there. At the same time, the concentration buildup in the three sections and in the cold box was logged. The section without vapor retarder (Section 2) showed a fast response. The section with the felt (Section 3) reacted slower, while the section with the polyethylene film (Section 1) demonstrated a tracer buildup as slow as in the cold box. After a period of time, however, all concentrations tended to the same value as maintained in the hot box. This underlined that no air from the laboratory entered the ridge, albeit there were some small leakages the other way around, from the hot box to the laboratory.

The related airflows were derived from a least-squares analysis on the logarithmic representation of the concentration buildup vs. time in the three sections and the cold box. By dividing the flows found that way by the air pressure differences measured in the three sections, the air permeances of the shingled decks and the inside linings, the last including the polyethylene film in Section 1 and the felt in Section 3, could be calculated (see Table 3).

TABLE 3
Airflows from the Hot Box to the Three Sections and Airflow through Parallel Leaks between the Hot and Cold Box. Air Permeance of Each of the Sections at the Hot and Cold Box Side

Hot Box → Roof → Cold Box	Airflow, m^3/h	Air Permeance Inside Lining, $kg/(m^2 \cdot Pa \cdot s)$	Air Permeance Shingled Deck, $kg/(m^2 \cdot Pa \cdot s)$
Roof 1	0.13	1.16×10^{-6}	2.9×10^{-6}
Roof 2	0.32	1.92×10^{-6}	3.2×10^{-5}
Roof 3	0.20	1.20×10^{-6}	1.1×10^{-5}
Hot Box → Cold Box in Total	3.32	—	—

Table 3 makes it clear that some direct air leakage exists between the hot and the cold box. Although the related airflow was very low, only 2.67 m^3 per hour, this path was far more important than the exfiltration through the three sections. Those rates were, in fact, insignificant, which indicates that the first requirement for a self-drying concept to eliminate vapor transfer by convection was matched very well by the test.

The inside lining of Section 2 (no vapor retarder) has an air permeance within the range of values, measured on individual gypsum boards. On the contrary, the inside lining of Section 3 has an air resistance that lies 1.5 times lower than the sum of the average air resistances of the felt and the gypsum board. Finally, in Section 1, the inside lining has an air permeance that is 26,000 times higher than the one measured on individual polyethylene film samples. This underlines that using an absolute airflow retarder is no guarantee for an airtight roof. In fact, the lower the initial air permeance of the retarder, the more impact small imperfections, such as perforations by stapling, and workmanship flaws have on the final result.

Moisture Performance of the Three Sections

Summer Conditions. Figure 3 lists the moisture ratio in the plywood deck, the moisture ratio in the two layers of

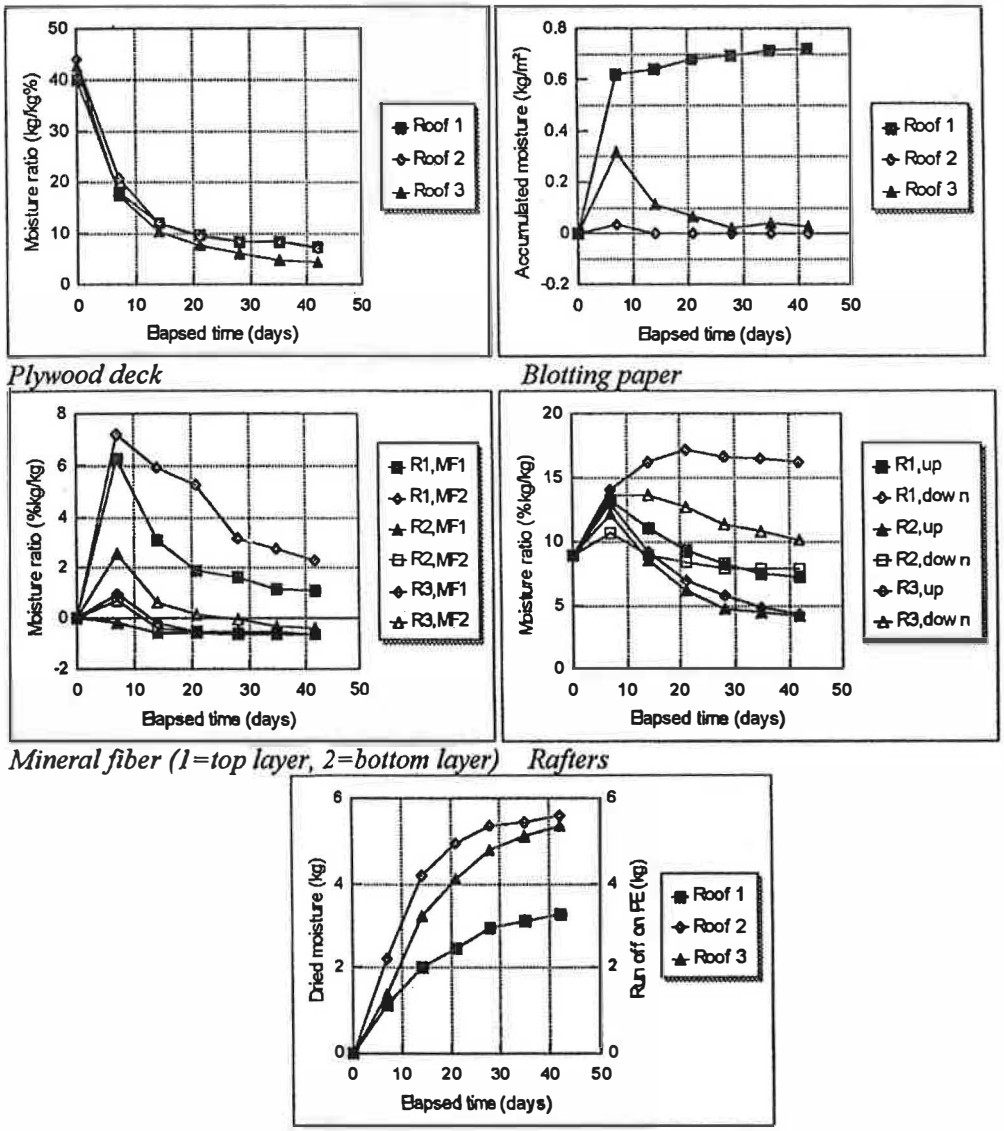

Figure 3 *Summer conditions, moisture ratio in the plywood, the blotting paper, the rafters and the mineral fiber, total dried (Sections 2 and 3) and condensed quantities (Section 1).*

mineral fiber, the moisture ratio in the central rafter, and the moisture quantity in the blotting paper.

Drying of the plywood only slightly differs between the three sections. Even the moisture ratio in the plywood at the end of the summer period is identical in the three sections. In the section with the polyethylene film (Section 1), however, the moisture ratio in the mineral fiber reaches the highest value. At the end of the summer period, the insulation layer there is also the wettest. The electrical measurements in the rafters of the three sections, just under the plywood, confirm the evolution of the moisture ratio, as measured in the loose-fill piece mounted there (see Figure 4). Hence, while the rafters in Sections 2 and 3 are dry over the entire height at the end of the summer period, they remain quite wet just above the polyethylene film in Section 1.

The largest difference in moisture performance between the three sections is seen in the humidity response of the blotting paper. In Section 1, moisture accumulates quickly in the blotting paper the first week. After that week, when the plywood has lost most of its built-in water, it slows down but never stops. This suggests a continuous water vapor diffusion from the plywood to the polyethylene film where it condenses. In Section 3, on the contrary, accumulation in the blotting paper peaks during the first week to decrease quickly from the second week. Complete dryness is reached at the end of week four. Finally in Section 2, the blotting paper shows a small humidity peak after week one but is already dry at the end of week two. Apparently, Sections 2 and 3 reach an air-dry state, although the transition from wet to dry takes some extra weeks in Section 3 (the one with the felt). Section 1, on the contrary, does not dry at all.

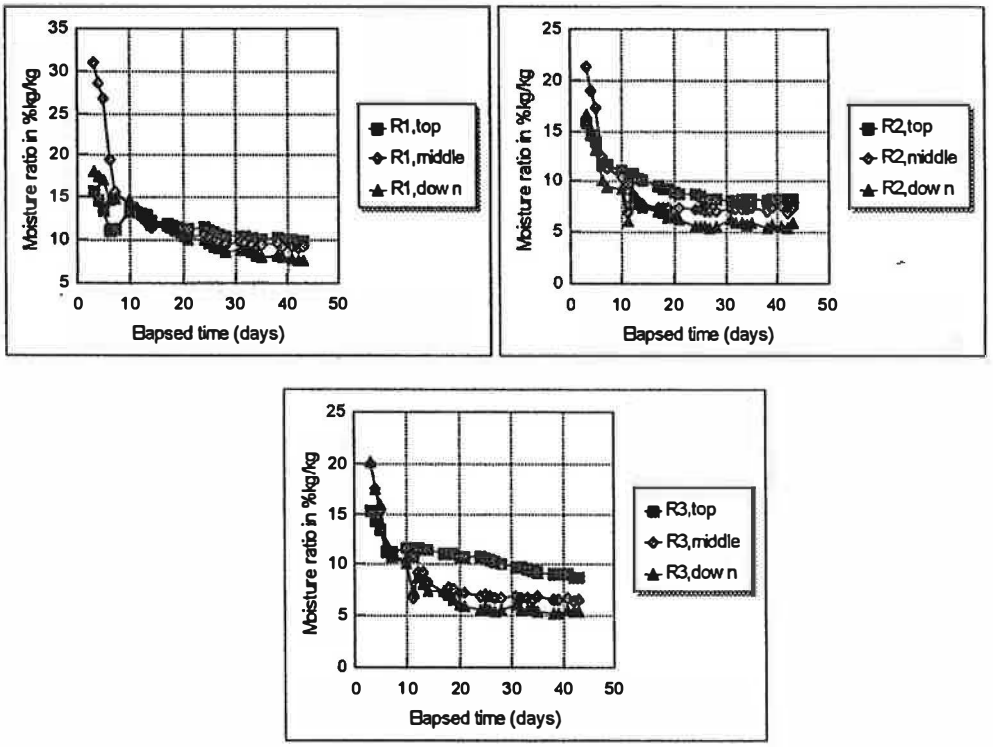

Figure 4 *Electrical measurements in the central rafters of the three sections.*

At the end of the summer period, Section 2 lost 5.6 kg of water: 4.75 kg from the plywood, the rest from the rafters. Section 3 lost 5.37 kg: 4.8 kg from the plywood, the rest from the rafters. In Section 1, 4.15 kg diffused from the plywood to the polyethylene film. Of that quantity, 0.08 kg condensed in the mineral fibre, 0.77 kg was absorbed by the rafters, and 0.03 kg was absorbed by the blotting paper. The rest, 3.27 kg, accumulated on the polyethylene film, where it ran off and wetted the thermal insulation and rafters at the bottom.

All of the estimates, of course, are approximate values, as moisture absorption in the three rafters of each section is based on an extrapolation of the measurements on two small loose-fill pieces in the central rafter. Also, only half the insulation was weighted and the results extrapolated for the whole volume of mineral fiber.

Winter Conditions. Moisture uptake by the plywood, the mineral fiber, the rafters, and the blotting paper in Sections 2 and 3 and total moisture accumulation in all parts of Section 1 are plotted in Figure 5.

In Sections 2 and 3, the moisture increase is caused by interstitial condensation. In Section 1, on the contrary, the moisture increase in the plywood is to a large extent due to a redistribution, by diffusion back to the plywood, of water condensed on the polyethylene film and run-off collected at the bottom of the section. Table 4 shows that both interstitial condensation and redistribution are far from one-dimensional. In fact, at the end of the winter period, moisture ratio in the deck of Section 1 reaches 30% by weight near the top, 15% by weight in the middle of the section, and 45% by weight at the bottom. In Sections 2 and 3, the top tends to be 20% per weight. The humidity gradient from top to bottom in the plywood deck of Section 3 is clearly linked to buoyancy-induced air circulation in and around the mineral fiber. This circulation also exists in Section 2. The higher vapor ingress from the hot box through the gypsum board, however, is masking it; see Table 5. Note that only 57% to 66% of the incoming water vapor condenses against and in the plywood deck. The rest is absorbed by the rafters and the mineral fiber. In global, Section 3 demonstrates a significantly lower vapor ingress by diffusion than Section 2.

Thermal Performances of the Three Sections

Summer Conditions. For a sunny test day, the average temperature profile in the sections is shown in Figure 6. The temperature between the plywood deck and shingles reaches 68.5°C. Underneath the plywood, 64.6°C is noted. Between both mineral fiber layers, temperature peaks at 45.8°C, while at the inside lining, there is hardly any noticeable deviation from 22°C. At the same time, the time shift increases from the shingles down to the inside lining. The temperature difference over the plywood peaks at 20°C after 40 minutes of irradiation.

As soon as irradiation starts, the heat flux between the plywood and the shingles increases to a peak of 23.3 W/m^2. Then follows a slow decrease, until irradiation is switched off and the accompanying transient moves through the roof, with an inversion of the heat flux at the plywood, down to −11.6 W/m^2. On the inside lining instead, the exponential increase is much slower, with a peak at the end of the irradiation period

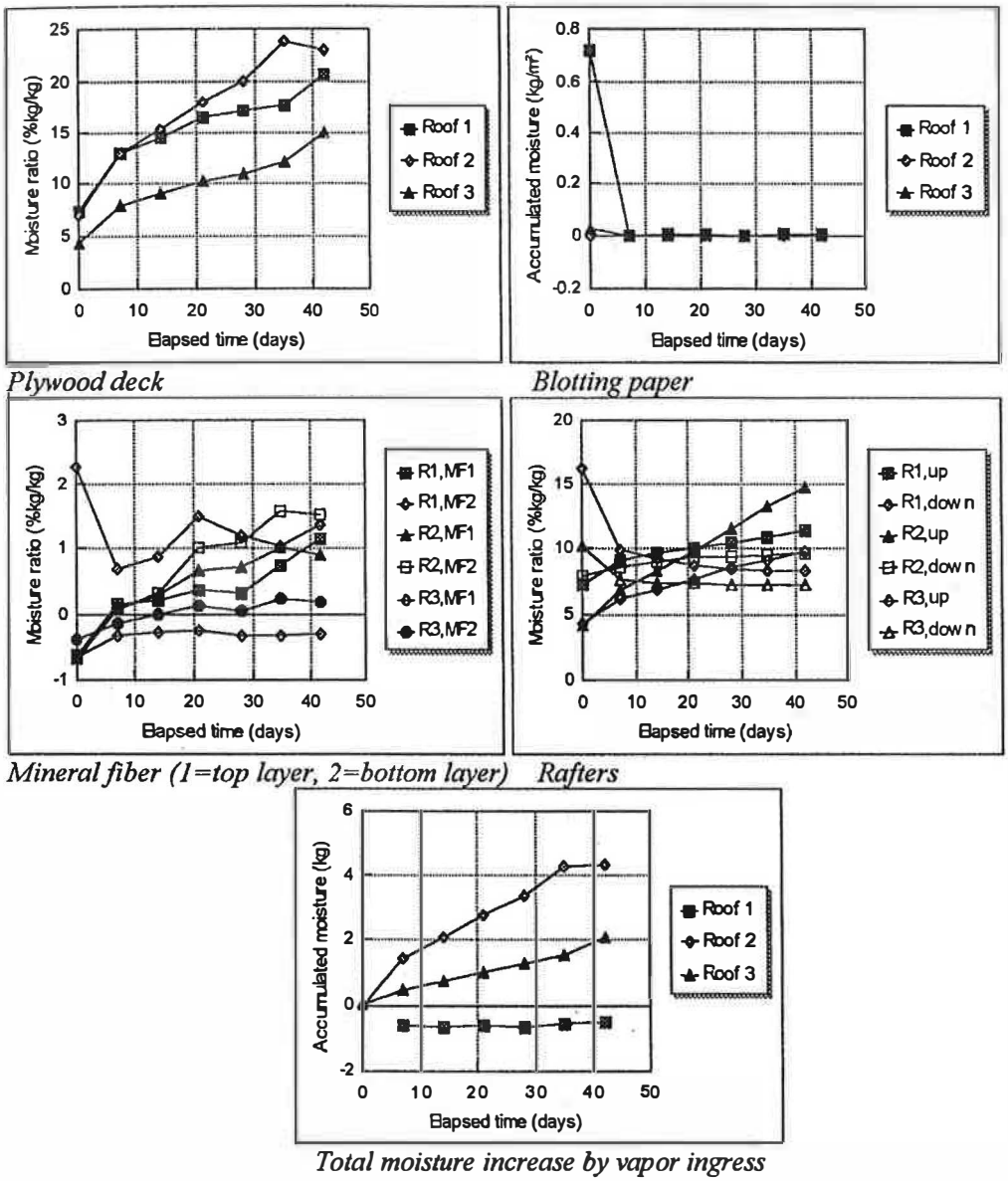

Figure 5 *Winter conditions, moisture ratio in the plywood, the blotting paper, the rafters, and the mineral fiber. Total moisture increase by diffusion and exfiltration.*

TABLE 4
Spot Moisture Ratios in Six Points of the Plywood Deck at the End of the Winter Period

	Section 1		Section 2		Section 3	
	Left	Right	Left	Right	Left	Right
Top	20.1	31.0	20.2	17.5	20.2	20.9
Middle	14.7	11.0	14.9	15.2	10.0	9.2
Bottom	22.4	45.0	15.4	19.2	7.4	7.2

TABLE 5
Overall Vapor Absorption and Condensation in Sections 2 and 3, Condensation in the Plywood Deck of Sections 1, 2, and 3

Section	Absorption + Condensation in the Section, kg/(m²·s)	Condensation in the Plywood Deck, kg/(m²·s)
1		2.2×10^{-7}
2	6.1×10^{-7} (2.21 kg/m² after 42 days)	3.5×10^{-7}
3	3.0×10^{-7} (1.09 kg/m² after 42 days)	2.0×10^{-7}

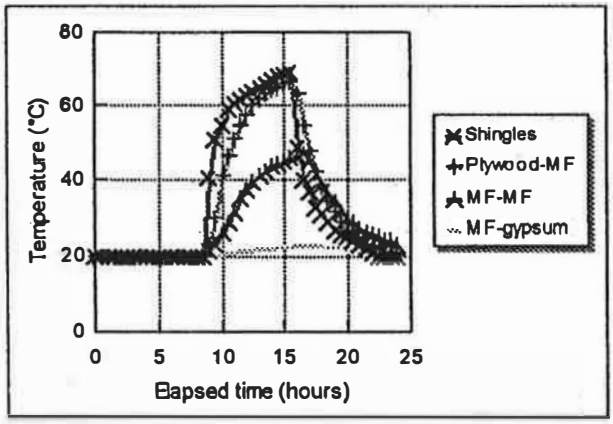

Figure 6 Temperatures in the sections during a summer test day.

of 26 W/m^2 followed by an exponential decrease to zero. The higher peak at the inside lining in comparison to the plywood shows that during irradiation, moisture evaporates at the plywood and moves to the inside lining where it condenses.

Winter Conditions. In winter, buoyancy-induced air circulation in and around the mineral fiber insulation affects the temperature profiles in the three sections in a rather moderate way. Also, the average heat fluxes at the inside and outside surface in all three roofs are nearly identical at –2.8 W/m^2 vs. –3.4 W/m^2, as calculated with conduction as the only transport mechanism. This small difference between the measured value and the calculated one is mainly caused by latent heat transfer. In fact, 0.6 W/m^2 indicates a condensation rate in the plywood of 2.4×10^{-7} kg/(m^2·s), i.e., close to the rates measured.

Conclusions from the Experiments

The experiments show that only Section 3 deserves the term "self drying." It has an acceptable airtightness, shows good drying behavior during the summer test period, and does not suffer from excessive interstitial condensation during the winter test period. Section 1, although the one with the highest airtightness and vapor tightness, suffers from summer condensation of built-in moisture against the polyethylene film, followed by winter condensation of the same moisture in the plywood deck and the rafters. Section 2 finally has an acceptable airtightness and the best drying response during the summer test period but shows excessive interstitial condensation during winter.

SIMULATION OF THE TEST RESULTS WITH SIMPLE AND SIMPLIFIED MODELS

In general, modeling has three objectives: (1) to get a better understanding of the test results and observations, (2) to extrapolate the test results to real climate conditions, and (3) to help in developing upgraded concepts. Hence, the main objective in this case was different. In fact, we liked to evaluate to what extent simple engineering tools and a simplified model could predict the hygrothermal response of each of the three-dimensional sections. Such type of evaluation does not lack importance. In fact, the use of full models, accounting for the whole three-dimensional geometry with all consequences for the heat, air, and moisture balance, is out of the question in most situations. The reasons for that are manifold: the whole three-dimensional geometry including all perforations, cracks, and flaws is an unknown reality beforehand; some of the consequences for the heat, air, and moisture responses are so complex that even full models cannot handle them accurately material data are never complete enough; time and money to do the full simulations are lacking; etc. Simple engineering tools and simplified models do not suffer from those inconveniences. Both consider a building element as being a one-dimensional system. Moreover, an engineering tool handles all material properties as constants. At the same time, it reduces the physics behind to some essentials: steady state heat conduction only, and neither latent heat transfer nor capillary moisture flow. A simplified model instead keeps track of all physical phenomena involved. It does that in a transient way. Material properties, however, are fitted into predefined functions of temperature, moisture ratio, and relative humidity.

Using Simple Engineering Tools

In winter conditions, interstitial condensation is analyzed using the dew-point method (ASHRAE 1997). A tool that convenes better for the winter test period in this particular case, however, is the convection, conduction, and diffusion model (CCD) (Hens 1996). In fact, the tracer gas measurements show that during the winter period, exfiltration intervenes. The test allowed us to quantify all airflows. The CCD model is based on a steady-state solution for combined heat conduction and enthalpy flow, respectively combined diffusion and vapor convection in the case of a one-dimensional geometry. Temperatures and vapor pressures in a section are given by

$$\theta_x = \theta - (\theta_i - \theta_e)(1 - \exp(c_a g_a R_{i,x}))/(1 - \exp(c_a g_a R_T)) \quad (1$$

$$p_x = p - (p_i - p_e)(1 - \exp(a_H g_a Z_{i,x}))/(1 - \exp(a_H g_a Z_T)) \quad (2$$

where g_a is the air flux in kg/(m^2·s), c_a is the specific heat capacity of air, R is the thermal resistance, and Z is the diffusion resistance. The suffix i refers to the inside, the suffix e to the outside, and the suffix T means total. The constant a_H which enters the equation through the conversion of vapor concentrations into vapor pressures (a_H equals the ratio between the gas constant for dry air and the product of the gas constant for water vapor and the atmospheric air pressure) has a value close to 6.21×10^{-6}.

The total heat flux by conduction and convection (q_T) and the total vapor flux by diffusion and convection (g_T), in turn, are expressed in terms of g_a, R_T, and Z_T by

$$q_T = c_a g_a[\theta_i - (\theta_i - \theta_e)/(1 - \exp(c_a g_a R_T))] , \quad (3)$$

$$g_T = a_H g_a[p - (p_i - p_e)/(1 - \exp(a_H g_a Z_T))] . \quad (4)$$

When the vapor pressure p_x, given by Equation 2, attains the vapor saturation pressure within the temperature range present in the section (see Equation 1), then concealed condensation is a fact. The condensation zone follows from the conservation of mass law. This law shows that not only the vapor and vapor saturation pressure but also their gradients should equal in each point of the condensation zone, including the beginning (x_1) and end of it (x_2). This leads to a total condensation rate between the points x_1 and x_2, given by

$$g_c = a_H g_a\{[p_i - (p_i - p_{sat,x2})/(1 - \exp(a_H g_a Z_{i,x2}))] - [p_{sat,x1} - (p_{sat,x1} - p_e)/(1 - \exp(a_H g_a Z_{x1,e}))]\} \quad (5)$$

with $Z_{i,x2}$, the vapor diffusion resistance between the end x_2 and inside, and $Z_{x1,e}$, the vapor diffusion resistance between the beginning x_1 and outside. In most cases, x_1 and x_2 coincide at one interface.

Boundary conditions for the calculations in this case were: $\theta_e = 2°C$, $\phi_e = 90\%$, $\theta_i = 22°C$, $\phi_i = 50\%$, measured exfiltration rates. Table 6 mentions the constant material properties. In the table, μ represents the diffusion resistance factor. Table 7 gives the results of both a CCD and dew-point calculation in confrontation with the measured data. The total moisture uptake per week as well as the condensation rate in the plywood are listed. Because none of the simple engineering tools account for the sorption effects by the rafters and the mineral fiber, one should compare the calculated values with the total uptake, not with the condensation rate in the plywood.

In that case, CCD fits better with the measured data than the dew-point calculation does. So, although air exfiltration was minimal, its influence cannot be overlooked. The result for the section with the polyethylene film (Section 1), for example, suggests that part of the winter humidifying of the plywood came from vapor ingress from the hot box by exfiltration. Also, the higher the vapor resistance of the inside lining, the more exfiltration affects the condensation rate. Although the lowest exfiltration rate was measured in Section 1, it multiplies the condensation rate there with a factor of 100. In Sections 2 and 3 instead, multiplication remains restricted to 2.9 and 1.6, respectively.

One may question why the calculated condensation rate (kg/week) passes the measured weekly moisture uptake in Section 2 with 36%, while in Section 3 it remains 30% lower. The limited accuracy of all measured moisture accumulation data is one of the reasons. Errors up to 10% cannot be excluded. Another reason is that the vapor resistances of Table 6 are only known with limited accuracy. For the humidity-

TABLE 6
Material Properties

Layer	Properties				
	Thickness, m	Thermal Conductivity, W/(m·K)	Thermal Resistance, $m^2 \cdot K/W$	Diffusion Resistance Factor, –	Diffusion Resistance, m/s
Shingles	0.009	0.2	0.045		5.4×10^{11}
Plywood	0.0125	0.16	0.078	20	1.4×10^{9}
Mineral Fiber	0.2	0.034	5.85	1.2	1.3×10^{9}
PE-Foil (Section 1)	0.0002	0.2	—		7.2×10^{11}
Felt (Section 3)	0.0003	0.12	—	1257	2×10^{9}
Gypsum Board	0.0125		0.128	10.7	7.2×10^{8}

TABLE 7
Moisture Uptake by Sections 1, 2, and 3—Measured vs. Calculated Values

Section	Total Moisture Uptake, Measured Data (+Uncertainty)	Plywood Only, Measured Data	Interstitial Condensation, Calculated Values, kg/week (Compare with Total Moisture Uptake)	
	kg/week	kg/week	CCD	Dewpoint
1	—	(0.221)*	0.096	0.00098
2	0.619±0.062	0.353	0.846±0.048	0.292±0.03
3	0.303±0.030	0.204	0.233±0.036	0.146±0.015

* This result includes initial moisture as well as condensation of vapor released in the hot box.

controlled vapor retarder, for example, this accuracy is not better than ±10%. Even the air exfiltration rates are uncertain. The 95% probability interval of the rates, found by the least-squares analysis, is ±14% for Section 1, ±3.4% for Section 2, and ±24% for Section 3. These errors introduce the uncertainties on the measured and calculated data of Table 7. Of course, the last and perhaps most important reason is that both simple tools do not consider all phenomena governing the hygrothermal response of the three-dimensional sections.

During the summer stage, the hot box is not pressurized. This makes exfiltration zero and turns CCD into a dew-point calculation. The dew-point method, however, was not conceived to analyze situations where initial moisture intervenes and where outside conditions are highly transient. To get a result, the following simplifications were assumed: (1) the plywood keeps 100% RH until a moisture content of zero, (2) a constant cold box temperature, which gives the same mean saturation vapor pressure in the plywood as the transient sol-air temperature does, convenes for the calculations. This temperature was calculated as being 38.4°C, while the average shingle temperature during the six weeks of summer testing did not pass 30.3°C. The 8.1°C difference between both follows from the exponential relationship between temperature and vapor saturation pressure.

Figure 7 summarizes the results of the summer calculations for the three sections. The results are better than expected. Although straight instead of curved drying lines a found for the plywood, the tangent at time zero of t measured curves and the calculated straight lines all inters the time axis after 11.5 days. In Section 1, most of the moistu also remains enclosed, while in Section 2 it dries, and Section 3 it dries but only after a condensation transient in t felt. The calculated moisture accumulation on the polyeth ene film in Section 1 and in the felt in Section 3 neverthele overestimates the condensation rates there, as a comparis between the measured moisture accumulation in the blotti paper of Sections 1 and 3 shows. Neglecting the sorption pro erties of the rafters apparently makes these rates too pessim tic. In fact, the moisture absorbed by the rafters and the mine fiber explains at least part of the differences found between t calculated and the measured condensation rates.

Using a Simplified Model

A simplified model keeps track of all physics involv but exchanges the real material property relations for simp fied, fixed functions. A construction is considered as bei one-dimensional. This is a far-reaching simplification in th particular case, as it excludes sorption by the rafters, stac induced air circulation in and around the mineral fiber, a gravity flow down the polyethylene film in Section 1. We us the 'Hygran24' code (Hens 1996). This transient code consi

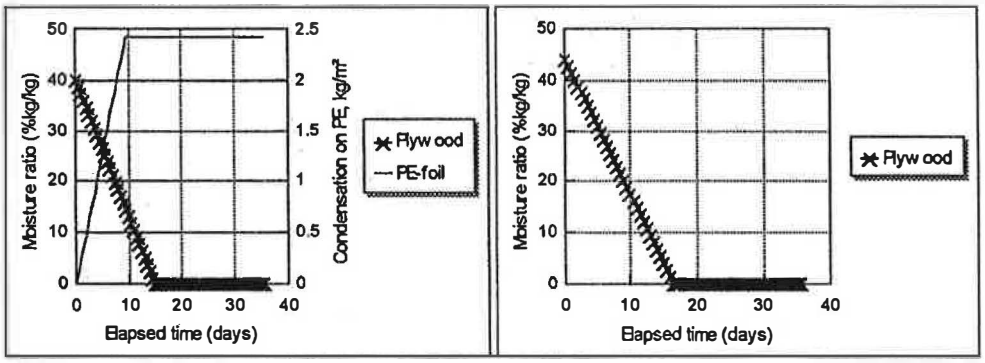

Section 1, plywood: drying curve. Polyethylene film: condensation curve

Section 2, plywood: drying curve, no condenstion in the gypsum board

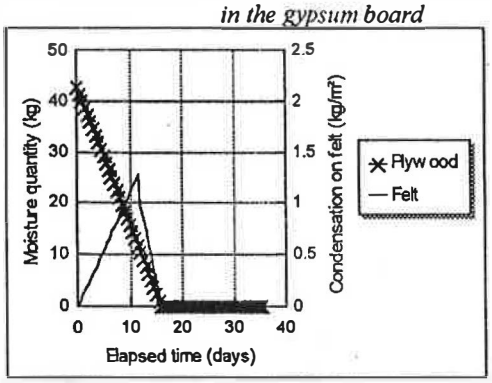

Section 3, plywood: drying curve, felt: wetting+drying curve

Figure 7 *Results of an enhanced dewpoint analysis for the summer situation.*

TABLE 8
Material Properties for Hygran24

Property	Plywood	Min.Fibre	PE-Foil	Felt	Gypsum
Thickness (cm)	1.25	20	0.02	0.03	1.25
Weight (kg/m²)			0.2	0.207	8.55
Density (kg/m³)	765	17.8			
Specific Heat Capacity (J/(kg·K))	1880	840	1470	1880	840
Dry Thermal Permeance (W/(m²·K)) Moisture Coeff. (W/(m²·K·%)			1000 0	400 7.4	7.84 0.145
Dry Thermal Conductivity (W/(m·K)) Moisture Coeff. (W/(m·K·%))	0.124 0.005	0.0342 5.7×10^{-6}			
Sorption Ratio at $\phi = 0.33$ (%kg/kg) Sorption Ratio at $\phi = 0.86$ (%kg/kg)	6.38 17.46			5.8 18.4	3.07 6.01
Capillary Moisture Ratio (%kg/kg)	75			108	58.4
Vapor Diffusion Thickness, RH_1 (m,%) Vapor Diffusion Thickness, RH_2 (m,%) Vapor Diffusion Thickness, RH_3 (m,%)			90	4.6, 26.6 0.215, 60.6 0.108, 91.8	0.158, 25 0.112, 65 0.066, 91
Vapor Resistance Factor, RH_1 (–,%) Vapor Resistance Factor, RH_2 (–,%) Vapor Resistance Factor, RH_3 (–,%)	168, 20 132, 60 16.8, 90	1.2			
Water Absorption Coeff. (kg/(m²·s$^{0.5}$))	0.003			0.00062	0.14
Air Permeance $K_a = (a\Delta P_a{}^b)$ a and b			2.9×10^{-6}, 0	3.2×10^{-6}, 0	1.9×10^{-6}, 0
Air Permeability, $(a\Delta P_a{}^b)$ a and b	3.74×10^{-3}	10^{-4}, 0			

ers combined heat, air, and vapor flow and phenomena such as sorption, latent heat transfer, and capillary water mitigation. Table 8 gives the code-specific property functions for plywood, mineral fiber, polyethylene film, cellulose felt, and gypsum board. Shingles are implemented as a constant vapor permeance of 1.85×10^{-12} kg/(m²·Pa·s) at the exterior surface. Thermal conductivity, in turn, is handled as a linear function of moisture ratio. Sorption is modeled starting from the moisture ratios at $\phi = 0.33$ and $\phi = 0.86$, respectively (ϕ: relative humidity in –). In fact, the code considers sorption as being a twofold linear reality, with the intersection between the two lines at $\phi = \phi_{threshold}$, with $\phi_{threshold}$ equaling 0.95 for capillary materials and 0.995 for noncapillary materials:

$$\begin{aligned} \phi \le \phi_{threshold} \quad & X_H = \frac{X_{86} - X_{33}}{0.53}(0.33 - \phi) + X_{33} \\ \phi_{threshold} < \phi \le 1 \quad & X_H = \frac{X_c - X_{threshold}}{1 - \phi_{threshold}}(1 - \phi) + X_{threshold} \end{aligned} \tag{6}$$

$X_{threshold}$, the moisture ratio at the threshold relative humidity $\phi = \phi_{threshold}$, is calculated with the first equation. In the second equation, X_c is the capillary moisture ratio. Vapor permeability and moisture diffusivity are given by

$$\delta_v = a + b\exp(c\phi), \tag{7}$$

$$D_w = 0.00674\left(\frac{A}{w_c}\right)^2 \exp\left(\frac{6.4w}{w_c}\right). \tag{8}$$

Figure 8 summarizes the calculation results for the plywood deck. From a qualitative point of view, the moisture performance resembles the measurements: a fast summer drying followed by a slower winter wetting. Contrary to the dew-point calculation, where drying gave a straight line, the curve found here follows the measured data.

From a numerical point of view, however, the calculations are disappointing. Summer drying of the plywood seems quite well estimated for Sections 1 and 3, but for Section 2 the moisture ratio decreases much slower than calculated. Predicted winter condensation in all three sections at the same time overestimates the measured moisture uptake by the plywood. There are different reasons for that. Some of the material properties were taken from literature. They may differ from the real values. The vapor permeability of the felt was modeled, using the code-related exponential function (Equation 7). Hence, detailed measurements found that a better relation would be the one listed in Table 1. This relation, however, cannot be handled by the simplified model. The Hygran24 model considers each section as being one-dimensional. In reality, they are three-dimensional. As a consequence, an important fraction of the incoming vapor is absorbed by the rafters. In the one-dimensional simulation, these rafters are omitted and that part of the vapor ingress also

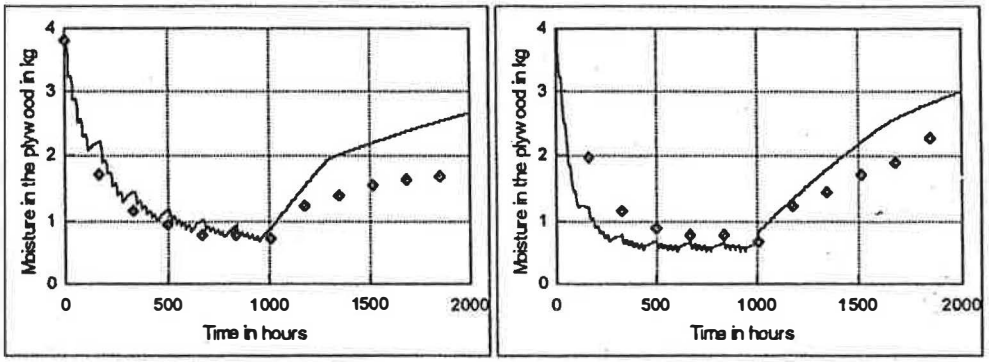

Section 1, with polyethylene film *Section 2, no vapor retarder*

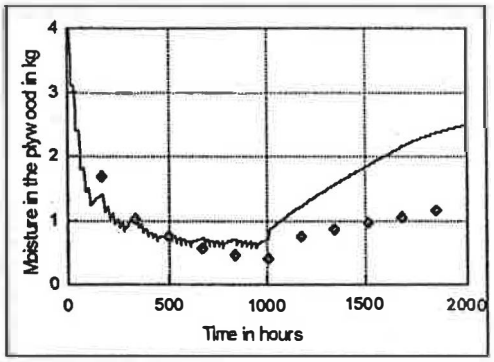

Section 3, with the felt

Figure 8 *Summer drying, followed by winter condensation: moisture accumulation in the plywood, measured (spots) vs. calculated data.*

condenses in the plywood. As a result, the calculations must overestimate moisture accumulation in it. If the same ratios as in the measurements are handed between the total moisture uptake in the sections and the part that condenses in the plywood, the overestimation reaches 45% in Section 2 and 34% in Section 3. Subtraction of those absorbed quantities from the calculated winter accumulation in the plywood brings the simulations much closer to the measurements. This underlines that simplifying the geometry with exclusion of important sorption masses distorts the numerical results and the conclusions drawn from it. In fact, if one had to decide on the effectiveness of the humidity-controlled vapor retarder based on the calculations, the conclusion would be negative. Drying of Section 3 looks good, but at the end of the 42-day winter period, a too high moisture ratio, up to 25% kg/kg, is found in the plywood. Of course, gypsum board without the felt behaves worse, with a moisture ratio up to 31.4%.

CONCLUSIONS

A comparative series of drying-condensation tests was set up on three sloped roof sections. These had shingles on plywood as a roof cover, a 20 cm thick mineral fiber insulation, and a gypsum board lining. Section 1 contained a polyethylene film as a vapor and airflow retarder between the mineral fiber and the inside gypsum board, while Section 3 got a new type of felt as a humidity-controlled vapor retarder. Section 2 included no retarder at all. Before the test started, the plywood deck was humidified to a moisture ratio of 38% to 44% kg/kg. During the first 42 days, summer drying was simulated. Sections 2 and 3 dried without causing any problem, while Section 1 demonstrated summer condensation against the polyethylene film. This ended in run-off, with severe wetting of the insulation and the rafters at the bottom of the section. During the next 42 days, average winter conditions were maintained. Sections 2 and 3 both underwent interstitial condensation. In Section 3, however, only half the amount of condensate detected in Section 2 was measured. In Section 1, diffusion directed the moisture from the polyethylene film back to the plywood, which was wetted to a degree only slightly different from Section 2. A major conclusion of the research, therefore, was that only Section 3 could deserve the term self-drying.

After the tests, an attempt was made to simulate the measurements using two simple engineering tools and one simplified model. One of the simple tools considered steady-state conduction, convection, and diffusion (CCD). The transient simplified model added sorption, capillary transport, and latent heat transfer to that but used fixed functions to describe the relations between properties and potentials. In both cases, the geometry is reduced to one-dimensional. For Sections 2 and 3, the CCD tool predicted condensation in winter quite well. Summer drying, however, demanded additional assump-

tions to make an approximate solution possible. On the contrary, the simplified model simulated the overall moisture performance of the plywood in a qualitatively correct way. Numerically, the results were less convincing. The drying curve in Section 2 was too steep, and in all three sections, predicted condensation in the plywood was larger than measured. The differences proved that by assuming a one-dimensional geometry and consequently omitting some important sorption masses, the simplified model performed rather poorly. One of the consequences, however, could have been that, if the new felt was evaluated on the basis of the simulations only, the conclusion should not have been that Section 3 (the one with the felt as airflow and vapor retarder) deserved the name self-drying. This led to a second conclusion: be careful with simple tools or simplified models when evaluating new developments. Although they seem scientific, they may overlook important realities that have a large impact on the hygrothermal response.

REFERENCES

ASHRAE. 1997. *1997 ASHRAE Handbook—Fundamentals*. Atlanta: American Society of Heating, Refrigerating and Air-Conditioning Engineers, Inc.

Cunningham, M.J., M.R. Bassett, D. McQuade, and M. Beckett. 1994. A field study of the moisture performance of roofs of occupied newly constructed timber framed houses. *Building and Environment* 29(2): 173-190.

Desjarlais, A. 1995. Self-drying roofs: What?! No dripping. *Proceedings of the Thermal Performance of the Exterior Envelopes of Buildings VI, Clearwater Beach, Florida, December 4-8*, pp. 763-773. Atlanta: American Society of Heating, Refrigerating and Air-Conditioning Engineers, Inc.

Hens, H., B. Remans, E. Vanmechelen, and M. Hus. 1992. Pitched roofs, heat-air-moisture transport in tiled and slated roofs with the thermal insulation at rafter level. Paper T4-B-92/01, *IEA-Annex 24*, 99 pp.

Hens, H. 1997. Hygric properties of a new humidity controlled vapor retarder. Paper presented at the CIB-W40 meeting, Kyoto.

Hens, H. 1996. Modeling. Final Report. *IEA-Annex 24*, Task 1, ACCO, Leuven, 90 pp.

Künzel, H., and Th. Grosskinsky. 1989. Untersuchungen über die Feuchigkeitsverhältnisse bei wärmegedämmten Satteldach-Konstruktionen. IBP-Bericht FB/1989, Holzkirchen, 14 pp.

Künzel, H.M., and Th. Grosskinsky. 1997. Feuchtebelastungen beeinträchtigen die Wirkung von Dampfbremspappen, Mitteilung 309, Fraunhofer Institut für Bauphysik.

Rose, W.B. 1994. Temperature and moisture content values from the attic performance project. Paper T4-US-94/02, *IEA-Annex 24*.

Rose, W.B. 1995. The history of attic ventilation regulation and research. *Proceedings of the Thermal Performance of the Exterior Envelopes of Buildings VI, Clearwater Beach, Florida, December 4-8*, pp. 125-134. Atlanta: American Society of Heating, Refrigerating and Air-Conditioning Engineers, Inc.

Sanders, C. 1996. IEA-Annex 24, Final Report, Volume 2, Task 2: Environmental conditions, Leuven, 96 pp.

TenWolde, A., and C. Carll. 1992. Effect of cavity ventilation on moisture in walls and roofs. *Proceedings of the Thermal Performance of the Exterior Envelopes of Buildings V, Clearwater Beach, Florida, December 7-10*, pp. 555-562. Atlanta: American Society of Heating, Refrigerating and Air-Conditioning Engineers, Inc.